Asociación Argentina
de Mecánica Computacional

Mecánica Computacional Vol XXXIV, págs. 3351-3367 (artículo completo)
Sebastián Giusti, Martín Pucheta y Mario Storti (Eds.)
Córdoba, 8-11 Noviembre 2016

INVERSION OF SEISMIC ANISOTROPIC PARAMETERS USING VERY FAST SIMULATED ANNEALING WITH APPLICATION TO MICROSEISMIC EVENT LOCATION

Daniel O. Pérez[1,2], Soledad R. Lagos[1], Danilo R. Velis[1] and Juan C. Soldo[2]

[1] *Facultad de Ciencias Astronómicas y Geofísicas, UNLP, La Plata; and CONICET, Argentina.*
dperez@fcaglp.unlp.edu.ar, slagos@fcaglp.unlp.edu.ar, velis@fcaglp.unlp.edu.ar

[2] *YPF Tecnología S.A., Argentina. juan.c.soldo@ypf.com*

Keywords: geophysics, VFSA, inversion, anisotropy, velocity calibration, microseismic

Abstract. The study and interpretation of hydraulically stimulated regions, such as certain unconventional hydrocarbon reservoirs (e.g. Vaca Muerta Formation, Neuquén, Argentina), requires the accurate location of the induced microseismic events. The localization is carried out by means of the analysis of the travel times of the generated compressional and shear seismic waves from the unknown event position to a set of geophones, usually located in a nearby monitoring well. The accuracy of the localization, and thus the characterization of the fracturing process, can be strongly affected by the available seismic velocity model, from which only estimates are known. Also, the underlying medium usually shows an anisotropic behavior, meaning that the velocities of the seismic waves depend on the propagation direction. Therefore, knowledge of the parameters that characterize the anisotropy and an appropriate calibration of the velocities can reduce the errors in the localization of the microseismic events. In this paper we propose a strategy to simultaneously calibrate the velocity model and invert the anisotropy parameters from three-component microseismic data. The strategy relies on the hypothesis that the subsurface is composed of a finite number of horizontal layers with weak anisotropy, a widely used approximation that requires only three anisotropy parameters per layer. The differences between the observed and the calculated travel times, for a known seismic source, are quantified by means of an appropriate objective function that turns out to be non-linear and multimodal. For this reason, we minimize it using very fast simulated annealing (VFSA), a stochastic global optimization algorithm devised to find near-optimal solutions to hard optimization problems. Tests on synthetic data show that the proposed strategy can be used to effectively calibrate the seismic velocities and to provide appropriate estimates of the anisotropy parameters in spite of the severe non-uniqueness of the inverse problem at hand. Also, the stochastic nature of VFSA allows us to obtain the uncertainties of the solutions by repeating the inversion several times. Finally, by means of a simulated microseismic location example, we show the importance of having a well calibrated model to successfully estimate the locations of the hydraulically induced events.

1 INTRODUCTION

Unconventional reservoirs, such as tight and shales, are mainly composed by intrinsically low permeability rocks, where hydrocarbon is isolated within fractures, microfractures and micropores making their exploitation difficult and expensive. In order to enhance production this type of reservoirs require hydraulic stimulation to create pathways connecting the isolated hydrocarbon with the well bore, increasing permeability. The pressure increment induced by the hydraulic stimulation can produce slippage along weakness planes in the reservoir rocks near the treatment well (Warpinski et al., 2005). The activation of pre-existing fractures and the creation of new ones produce microseismic activity and the consequent propagation of compressional and shear seismic waves (Lay and Wallace, 1995) which are recorded on geophones at the surface, shallow boreholes or nearby wells. The first-arrival times of these waves can be measured and the location of the aforementioned slippages can be inferred, given a velocity propagation model. This process is known as fracture mapping and allows to characterize how the fractures propagate through the reservoir rocks. The identification of fracture groups and their preferential direction is of paramount importance in the exploitation of the reservoir and in the planning of new exploration wells (Downton and Gray, 2006; Chen et al., 2012; Liu and Martinez, 2012; Mahmoudian et al., 2013; Bachrach, 2014; Maxwell, 2014). In addition, regarding the environmental concerns associated to the hydraulic fracturing, fracture mapping is a useful tool that provides information to avoid accidents such as shallow aquifer contamination or hydraulic fracturing-induced seismicity.

An accurate location of the microseismic events is necessary to correctly characterize the hydraulically stimulated region. The uncertainty associated with the location has several causes. One cause is the inability to accurately detect the compressional and shear phase arrivals at a sufficient number of receivers, because the number of geophones is often very limited and the coverage is poor. Another cause is the difficulty to adequately determine the velocities at which the seismic waves propagate through the medium (Warpinski et al., 2005). The seismic velocities within a reservoir are affected by numerous parameters such as the porosity, fluid content, pressure, and temperature. In addition, the underlying medium often shows an anisotropic behavior, meaning that the velocities of the seismic waves depend on the propagation direction. The location also depends on the signal-to-noise ratio of the data. As the quality of the data decreases, also does the accuracy of the first-arrival picking.

Usually the estimation of the velocity model begins with a low frequency geologically suitable earth model, which is improved using high frequency values from a dipole sonic log at a nearby well. Most common logging tools only measure vertical velocities and their use can lead to large errors in the location of the microseismic events, because these values are not reliable away from the well (Maxwell et al., 2010). To improve the results it is necessary to calibrate the model using additional information. This calibration is usually done by means of a calibration shot, for example a perforation shot, a string shot or a drop ball. Unlike the microseismic events, the location of the calibration shot is well known, and the calibration can be carried out by solving an inverse problem with non-unique solution (Akram and Eaton, 2013). On the other hand, logging tools do not provide enough information to accurately characterize anisotropy, a property that most sedimentary rocks exhibit at a significant degree. Anisotropy can be consequence of many complex factors such as natural fractures in the geological formations, alignment in the crystalline structure of the minerals in the rocks and thin layer structures in the subsurface. A correct characterization of the subsurface anisotropy and a precise velocity calibration will improve the microseismic location. Also, depletion-induced pressure drop and

pore-fluid changes may occur, affecting the velocities, if the reservoir has been exploited for a long time. Hence, a re-calibration just before commencing fracture mapping is sometimes necessary.

In this work we propose a strategy to calibrate the velocity model and to simultaneously estimate the anisotropy parameters from three-component microseismic data. The strategy relies on the hypothesis that the subsurface is composed of a finite number of horizontal layers of known thickness and vertical transverse isotropic behavior (VTI) (Tsvankin and Grechka, 2011; Tsvankin, 2012). Moreover, we are going to assume "weak" anisotropy (Thomsen, 1986), a widely used approximation that leads to only three anisotropy parameters per layer (Thomsen parameters). Given a known seismic source, the differences between the observed and the calculated traveltimes are quantified by means of an appropriate objective function. To this end, we developed a very efficient ray tracing algorithm that allows to calculate the traveltimes from the source to the geophones for any given layered VTI velocity model. The ray tracing algorithm is designed to work with any number of sources and geophones located in any position within the model limits. The aforementioned objective function thus depends on the compressional and shear vertical velocities, and the Thomsen parameters of each layer. Because of the layering and the way that the various parameters affect the traveltime calculations, the resulting cost function is discontinuous, non-linear and multimodal, thus requiring the use of a global optimization algorithm to avoid local minima and convergence issues. In this work we use very fast simulated annealing (VFSA) (Ingber, 1989), a stochastic global optimization algorithm devised to find near-optimal solutions to hard optimization problems. One advantage of using an stochastic algorithm such as VFSA is that the uncertainty of the solutions can be estimated, exploiting the large number of solutions that are tested during the inversion process.

Several authors have developed methods to calibrate isotropic and anisotropic velocity models with very interesting and useful results. Warpinski et al. (2005) and Pei et al. (2009) estimate horizontally layered isotropic velocity models from perforation shots. The former authors use multiple linear regression to build a system of equations from where the various parameters are obtained, while the latter authors use VFSA as in this work. Bardainne and Gaucher (2010) solve the eikonal equation and use simulated annealing to constrain isotropic velocity models with dipping interfaces and velocity gradients. Pei et al. (2014) and Li et al. (2014) propose to use the Levemberg-Marquardt algorithm to solve a linearized inversion scheme. The former to only estimate VTI models, and the latter to also estimate, given enough *a priori* information, the locations of the microseismic events.

This paper is organized as follows. First, we introduce the necessary theoretical background and make a detailed description of the inversion strategy. Next, we test the method on noisy synthetic microseismic data. The first two numerical examples show that the proposed strategy is capable of obtaining satisfactory results, allowing to obtain a good calibration of the velocities and an appropriate estimation of the Thomsen parameters, even when no *a priori* information about the anisotropy of the medium is available. In a third numerical example we show the impact of the uncertainties of the estimated models on the localization of microseismic events. Finally, a Conclusions section summarizes the obtained results. In the Appendix we provide a description of VFSA.

2 THEORY

2.1 Anisotropy

Sedimentary rocks in the subsurface often exhibit significant anisotropy in relation to the wave propagation velocities; that is, the velocities depend on the direction of propagation. In addition to the anisotropy, the subsurface is usually heterogeneous, making the velocities also dependent on the spatial position. Also, effective anisotropy and heterogeneity may be related. Anisotropy suggests certain structure on the scale of seismic wavelength and can be associated to various physical phenomena, such as the preferred orientation of minerals grains, the bedding of isotropic fine layers or the presence of vertical or dipping fractures and micro-cracks. As a consequence of the aforementioned factors, formations may have several anisotropic symmetries, leading to triclinic, monoclinic, orthorhombic or hexagonal media, among others (Tsvankin, 2012).

The inversion strategy proposed in this work is based on the hypothesis that the subsurface is composed of a finite number of homogeneous horizontal layers of known thickness, showing vertical transverse isotropic (VTI). Both anisotropy and heterogeneity are scale-dependent, then a medium can behave homogeneous for large wavelengths or isotropic for small wavelengths. Based on impedance well log information, one may argue that the real structure of the subsurface is continuous rather than layered (Cooke and Schneider, 1983). Nevertheless, it is known from well log data studies that the amplitudes of the reflection coefficients associated with the interfaces follow a non-Gaussian distribution (Walden and Hosken, 1986; Velis, 2003). This fact indicates that the main lithological units can be represented by layers with certain properties. In VTI media, which are a particular case of the anisotropy hexagonal media, there exists a single vertical axis of rotational symmetry, and the velocities only depend on the angle between the propagation direction and the symmetry axis. Every plane that contains the symmetry axis is a plane of mirror symmetry. The planes perpendicular to the symmetry axis are known as isotropy planes. Also, anisotropic media exhibit splitting or bi-refringence of the shear wave (Yilmaz, 2001), meaning that the shear wave is separated into two components or modes with different velocities: a slow- and a fast-shear wave with orthogonal polarizations. Then, when analyzing wave propagation in VTI media, one compressional wave and two shear waves must be considered.

2.2 Weak anisotropy

To characterize VTI media only five independent parameters are necessary (Backus, 1962; Berryman, 1979; Thomsen, 1986; Yilmaz, 2001). The most basic representation of these parameters are the five independent elastic constants of the stiffness tensor derived from Hooke's law (Aki and Richards, 1980; Lay and Wallace, 1995). This representation leads to seismic velocities equations that make difficult the development of inversion algorithms, and challenge the qualitative estimation of the effects of the anisotropy. To overcome these drawbacks, Thomsen (1986) redefined the anisotropy parameters obtaining the following expressions:

$$V_P(\theta) = V_{P0}(1 + \delta \sin^2\theta \cos^2\theta + \epsilon \sin^4\theta), \tag{1}$$

$$V_{SV}(\theta) = V_{S0}\left(1 + \frac{V_{P0}^2}{V_{S0}^2}(\epsilon - \delta)\sin^2\theta\cos^2\theta\right), \tag{2}$$

$$V_{SH}(\theta) = V_{S0}(1 + \gamma \sin^2\theta), \tag{3}$$

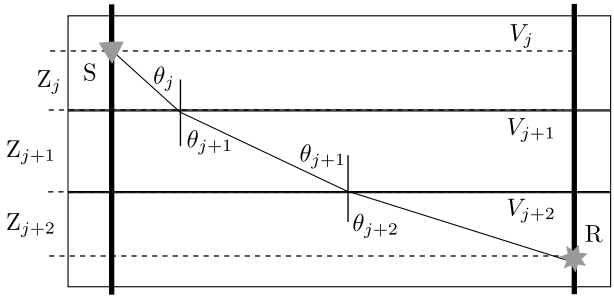

Figure 1: Single raypath for a layered homogeneous anisotropic velocity model.

where V_P is the compressional or P-wave velocity, V_{SV} and V_{SH} are the slow-shear or SV- and fast-shear or SH-wave velocities, respectively, and θ is the angle between the propagation direction and the symmetry axis, which in VTI media is vertical. In addition, ϵ, δ and γ are the so-called Thomsen parameters, which are dimensionless, while V_{P0} and V_{S0} denote the corresponding P- and S-wave vertical velocities.

The above equations are arranged so as to easily understand the effect of each anisotropy parameter on the seismic velocities (Berryman et al., 1999; Djikpesse, 2015). For waves propagating in the horizontal direction, i.e. angles near 90° with respect to the symmetry axis, V_P is principally affected by the parameter ϵ while V_{SH} by γ. The parameter δ also affects V_P, but to a lesser extent than ϵ. Due to its poor sensitivity to waves that propagate at horizontal directions, it is challenging to estimate δ from single-well sonic logging. The parameter δ controls V_{SV} for angles near 45°. Ultrasonic measurements in laboratory and field data measurements of velocities at seismic frequencies show that the anisotropy of sedimentary rocks is in the weak-to-moderate range, leading to anisotropy parameters with magnitudes usually much less than 0.2. Actually, equations (1) to (3) were derived assuming weak anisotropy, considering small values of ϵ, δ and γ. Even so, these equations and the Thomsen parameters are useful to describe general cases of VTI. It is worth notice that when $\epsilon = \delta = \gamma = 0$, then $V_P = V_{P0}$ and $V_{SV} = V_{SH} = V_{S0}$ for all values of θ, which corresponds to an isotropic medium.

2.3 Forward problem

Given a VTI medium, the traveltime calculation from a seismic source to a receiver is *per se* a non-linear inverse problem that requires the use of iterative methods. A seismic wave propagating in a given direction can be represented by a straight ray because the velocity is constant in that direction. For a velocity model composed of N_L homogeneous horizontal layers (Figure 1), the traveltime t from source S to receiver R for any given phase, can be calculated as the sum of the partial traveltimes within each layer. Then

$$t = \sum_{j=1}^{N_L} \frac{Z_j}{V_j(\theta_j)\cos(\theta_j)}, \tag{4}$$

where $V_j(\theta)$ and Z_j are the wave velocity and equivalent thickness (Yue and Xiao-fei, 2005), respectively, within layer j. The angle θ_j is the corresponding incidence angle, as shown in Figure 1. In the case of VTI media and weak anisotropy, $V_j(\theta_j)$ should be replaced by either $V_{Pj}(\theta_j)$, $V_{SVj}(\theta_j)$ or $V_{SHj}(\theta_j)$, depending on the phase arrival whose traveltime (and trajectory) is to be calculated.

In an horizontally layered medium any seismic raypath must obey Snell's law (Aki and Richards, 1980; Lay and Wallace, 1995) or, equivalently, Fermat's principle (Sheriff, 2002).

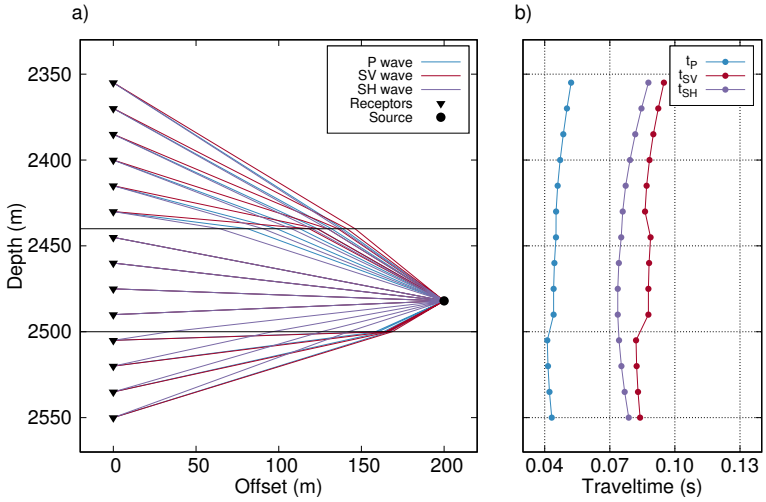

Figure 2: a) Raypaths and b) traveltimes for compressional and shear waves for the model described in Table 1.

Interface depth (m)	V_{P0} (m/s)	V_{S0} (m/s)	ϵ	δ	γ
——— 2440 ———	4290	2530	0.143	0.120	0.125
——— 2500 ———	3633	2280	0.249	0.190	0.192
	4289	2529	0.130	0.130	0.070

Table 1: Vertical velocities and Thomsen parameters used to calculate the raypaths and traveltimes depicted Figure 2.

This principle establishes that the traveltime of any seismic raypath is minimum (actually, stationary) as compared to any neighboring path, and so the first-order variation of the traveltime with respect to the neighboring paths must be zero. Then, all we have to do is to minimize equation (4) with respect to θ_j, $j = 1, N_L$. We solve the resulting equations, which are non-linear, iteratively by means of the conjugate gradient method.

As an example, Figure 2 shows the raypaths and the traveltimes t_P, t_{SV} and t_{SH} of the waves arriving at a vertical array with 14 geophones that span a depth range of 210 meters, 200 meters away from the seismic source. The model properties are described in Table 1.

At this point is important to notice that, in practice, the actual arrival times T of each wave-phase is given by the traveltimes t plus the origin time T_0 of the seismic event (e.g. calibration shot):

$$T_p = T_0 + t_P, \quad T_{SV} = T_0 + t_{SV}, \quad T_{SH} = T_0 + t_{SH}. \tag{5}$$

Naturally, in order to minimize inaccuracies in the estimated model and in the localization of the microseimic events (Warpinski et al., 2005), errors in T_0 must be kept to a minimum.

2.4 Inverse problem

Given a seismic source and an array of geophones, both with known positions, we want to determine the properties of the medium from the recorded arrival times of P-, SV- and SH-waves. This inverse problem involves the calibration of the vertical velocities and the estimation of Thomsen parameters. The origin time T_0 is assumed to be known. The inversion is carried out by minimizing the misfit between observed and calculated arrival times for the three phases. To

this end, we define the following cost function:

$$\Phi(\boldsymbol{V}_{P0}, \boldsymbol{V}_{S0}, \boldsymbol{\epsilon}, \boldsymbol{\delta}, \boldsymbol{\gamma}) = \left[\frac{1}{N_S N_R} \left(\|\boldsymbol{t}_P^{cal} - \boldsymbol{t}_P^{obs}\|_2^2 + \|\boldsymbol{t}_{SV}^{cal} - \boldsymbol{t}_{SV}^{obs}\|_2^2 + \|\boldsymbol{t}_{SH}^{cal} - \boldsymbol{t}_{SH}^{obs}\|_2^2 \right) \right]^{1/2}, \quad (6)$$

where N_S and N_R are the number of seismic sources and receivers, $\boldsymbol{V}_{P0}, \boldsymbol{V}_{S0}, \boldsymbol{\epsilon}, \boldsymbol{\delta}$ and $\boldsymbol{\gamma}$ are vectors of dimension N_L representing the vertical velocities and Thomsen parameters, and $\boldsymbol{t}^{cal}$ and $\boldsymbol{t}^{obs}$ are vectors of dimension N_R representing the calculated and observed arrival times for the P-, SV- and SH-waves, respectively.

Since Φ is discontinuous, multimodal and highly non-linear with respect to the unknowns $\boldsymbol{V_{P0}}, \boldsymbol{V_{S0}}, \boldsymbol{\epsilon}, \boldsymbol{\delta}$ and $\boldsymbol{\gamma}$, we minimize it using a global optimization algorithm. In particular, we use very fast simulated annealing (VFSA), which does not require the use of gradients or derivatives, avoids local minima and converges fairly fast. One advantage of using VFSA is its stochastic nature, that allows to calculate the uncertainties in the estimated solutions. Also, the restriction of the search space, whenever the available *a priori* information dictates it, is straightforward. In Appendix B we give a detailed description of VFSA.

It is worth noticing that the proposed cost function implies that the differences between the observed and calculated times follow a Gaussian distribution (Sivia, 1996). These differences have several causes. One cause is given by the errors associated with the models and algorithms used to calculate the arrival times. These errors can be decreased by using complex model and raypaths parametrizations, but this may lead to impractical and computationally expensive algorithms. Other causes include the noise always present in the observed data, that has a direct impact on the reliability of the estimated solutions, and errors in the picking process used to determine the arrival times from the observed data (Akram and Eaton, 2016). Usually, when working with microseismic events, the picking is performed automatically due to the large amount of available data (Sabbione and Velis, 2012, 2013; Velis et al., 2015).

From a probabilistic point of view, given a certain tolerance misfit between observed and calculated arrival times, the set of parameters ($\boldsymbol{V_{P0}}, \boldsymbol{V_{S0}}, \boldsymbol{\epsilon}, \boldsymbol{\delta}$ and $\boldsymbol{\gamma}$) that globally minimizes the cost function Φ represents the most probable model (Tarantola, 2005). Assuming that the main source of errors is the picking process, then,

$$E\left\{\|\boldsymbol{t}^{cal} - \boldsymbol{t}^{obs}\|_2^2\right\} = \sum_{i=1}^{N_S} \sum_{i=1}^{N_R} e_{i,j}^2, \quad (7)$$

where $E\{\cdot\}$ is the expectation operator and $e_{i,j}$ the picking error for each source-receiver pair. Then, considering the same error for all source-receiver pairs, Φ is expected to attain a maximum value of

$$\Phi_{max} = \sqrt{3} k \Delta s, \quad (8)$$

where Δs is the sampling interval and k is an integer (number of samples) that represents the quality of the picking process.

3 NUMERICAL EXAMPLES

In this section we test the proposed algorithm by means of synthetic data examples. The data consist on the traveltimes for the P-, SV- and SH-waves calculated for the model shown in Figure 3. The model comprises four layers that represent main lithological units (black lines),

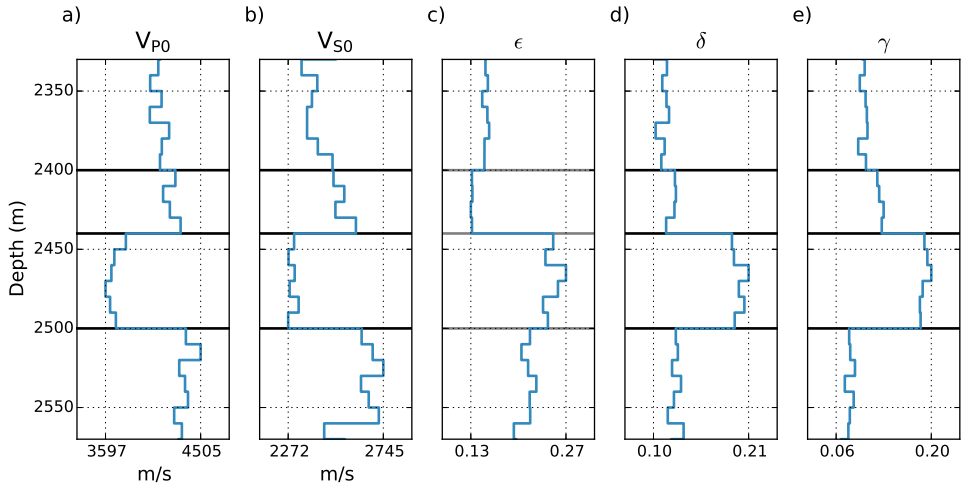

Figure 3: Layered model of vertical velocities and Thomsen anisotropy parameters corresponding to the model described in Table 2.

Interface depth (m)	V_{P0} (m/s)	V_{S0} (m/s)	ϵ	δ	γ
——— 2400 ———	4100	2400	0.150	0.110	0.100
——— 2440 ———	4290	2530	0.150	0.110	0.100
——— 2500 ———	3633	2280	0.249	0.190	0.192
	4381	2683	0.200	0.125	0.070

Table 2: Vertical velocities and Thomsen parameters used to generate the model shown in Figure 3.

plus a number of thinner layers (blue lines). The properties of the main units are summarized in Table 2. The model is based on the lithology of typical shale gas reservoirs such as the Barnett Shale of the Fort Worth Basin in Texas (Maxwell, 2009). The reservoir, which corresponds to the third layer, exhibits relatively low velocities, with faster units above and below. The thin layers depicted in Figure 3 represent model inaccuracies devised to simulate a more realistic scenario, for the inversion will be carried out by assuming four layer only.

For the inversion, we simulate two calibration shots by placing seismic sources at depths 2355 m (source S1) and 2480 m (source S2), 200 m away from a vertical monitoring well, as illustrated in Figure 4a. The receiver array is composed of 14 equispaced geophones spanning a range of 210 meters. Figure 4a shows the corresponding raypaths of the P-, SV- and SH-waves. The horizontal black lines represent the interfaces of the four main layers. Though the thin layers are not displayed, their effect on the raypaths are clearly visible. The corresponding traveltimes depicted in Figures 4b-c also are also affected by the thin layering. Since we are going to perform the inversion considering the main layers only, inaccuracies in the estimated magnitudes are expected. Regarding the error associated with the picking process, we are going to assume for all receivers an error of $k = 3$ samples, with an interval sampling of $\Delta s = 0.25$ ms. Then, following equation (8) we can accept solutions within a tolerance $\Phi_{max} = 1.29$ ms.

The search ranges of the velocities and Thomsen parameters of the four layers are given in Table 3. The interfaces depths are fixed. As the vertical velocities only need to be calibrated, we choose their search ranges relatively small. For statistical purposes, the inversion will be performed 100 times using different seeds for the annealing process. As stopping criterion, the inversion process will conclude whenever the misfit (6) is smaller than Φ_{max}. The final solution will be the mean of the 100 solutions.

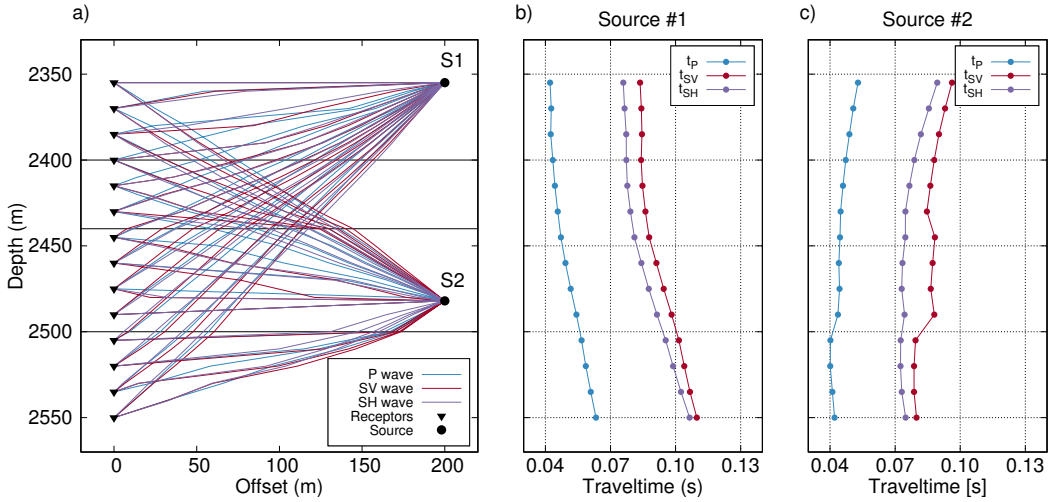

Figure 4: a) Raypaths for the model shown in Figure 3, and traveltimes corresponding to sources b) S1 and c) S2.

Interface depth (m)	V_{P0} (m/s)	V_{S0} (m/s)	ϵ	δ	γ
——— 2400 ———	3200 - 4800	1760 - 2640	0 - 0.2	0 - 0.3	0 - 0.3
——— 2440 ———	3350 - 5020	1785 - 2670	0 - 0.2	0 - 0.3	0 - 0.3
——— 2250 ———	2750 - 4120	2060 - 3100	0 - 0.3	0 - 0.3	0 - 0.3
	3420 - 5140	2300 - 3460	0 - 0.3	0 - 0.3	0 - 0.2

Table 3: Search ranges of vertical velocities and Thomsen parameters used in the inversion process.

3.1 First example: one source

In the first numerical example we only use the traveltimes shown in Figure 4c, which are calculated using the deepest source S2. The results of the inversion are shown in Figure 5. The curves represent the actual model (blue), the mean of the 100 realizations (red), and the standard deviation (gray areas). We observe that the mean calibrated velocities honor the actual values very accurately, while their standard deviations are relatively small, except for the shear wave of the first layer. These uncertainties are a direct consequence of the poor raypath coverage and the predominant direction of the rays arriving to the receivers placed within the first layer. In effect, when the incidence angles are nearly horizontal, the vertical velocities are only affected by ϵ and γ (see equations (1) to (3)). On the other hand, for oblique incidence angles, the vertical velocities are affected by the three Thomsen parameters, increasing the non-uniqueness (and the standard deviations) of the estimated magnitudes.

Regarding the Thomsen parameters estimates, a first look at the results shown in Figures 5c-d indicates that they are less accurate than those corresponding to the vertical velocities, except for γ in the third and four layers. This behavior is expected, because the relationships between the anisotropy parameters and the traveltimes (equations (1) to (3)) are rather ambiguous. Also, unlike the vertical velocities, the search ranges for these parameters are relatively large. The estimated ϵ honors the actual one very accurately, while its standard deviation is acceptable for all layers (Figure 5c). Contrarily, the estimated δ is the most inaccurate of all (Figure 5d), with large standard deviations for all layers, and a failure to capture the actual value for the reservoir layer. These results are expected, since traveltimes are little sensitive to δ. In the case of γ (Figure 5e), while the mean solution accurately follows the actual values for all layers, the standard deviation exhibits two distinct behaviors. It is large for the two first layers, and small

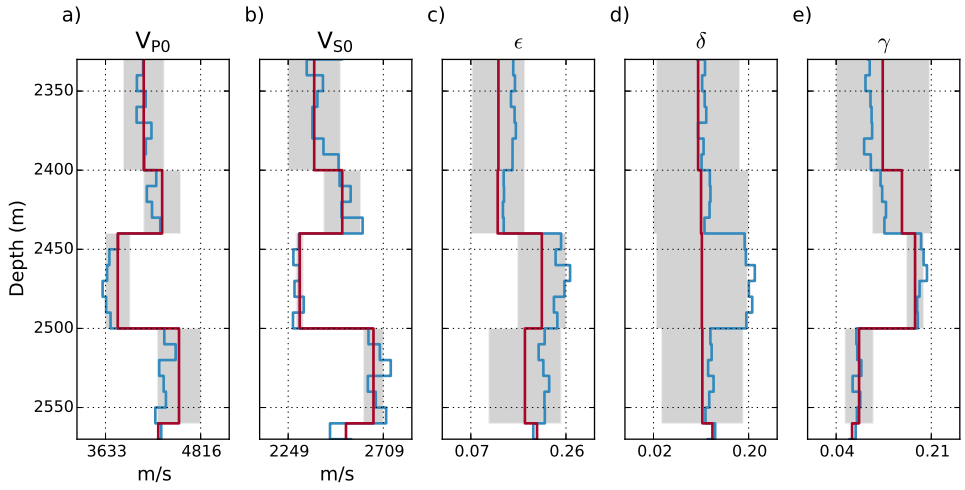

Figure 5: One source example. Estimated values for a) P-wave vertical velocity. b) S-wave vertical velocity, c) to e) Thomsen parameters ϵ, δ, and γ. Blue lines represent the actual model, red lines the mean value after 100 annealing iterations, and the shaded areas the standard deviation.

for the next two. This can be explained by the obliquity of the rays arriving to the receivers placed within the top two layers. As the incidence angle of the arriving rays decrease, also does the effect that γ has on the SH-wave velocity, increasing the non-uniqueness of this parameter. On the other hand, for near horizontal raypaths (third and fourth layers), the standard deviations are small.

3.2 Second example: two sources

In the second numerical example we use both traveltimes shown in Figure 4b and c, which are calculated using sources S1 and S2. The source S1, located at a shallower depth than source S2, not only provides extra information through the traveltimes, but also allows a wider incidence angle range at each receiver. Figure 6 shows the results of the inversion. A comparison with the results obtained in the previous example shows that the estimated solutions experienced a significant reduction of their standard deviations, especially for the vertical velocities and the Thomsen parameter γ, as shown in Figures 6a,b and e. The standard deviation of the latter is now small for all layers. This improvement is due to the almost horizontal rays that now arrive to the receivers located in the upper layers. Figure 6c shows that there is also a slightly improvement in the mean value of the parameter ϵ and the standard deviation of the upper layers. The additional data reduces the non-uniqueness of the solutions. Even so, the improvement in the solution for the parameter δ is negligible, the mean values are still not acceptable and the standard deviations only show a slight reduction, as shown in Figure 6d. A correct estimation of this parameter requires the use of additional information and constraints not contained in the arrival time observations.

3.3 Third example: event location

As explained before, errors in the velocity model are one of the main causes of uncertainty in the location of microseismic events. This 3D numerical example means to illustrate that situation.

Given a calibrated velocity model, the localization of the microseismic events is carried out

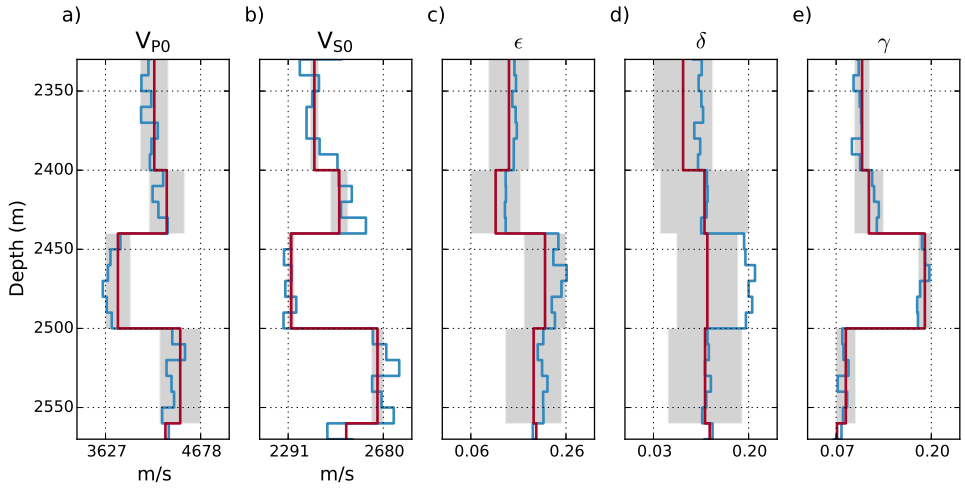

Figure 6: Two sources example. Estimated values for a) P-wave vertical velocity. b) S-wave vertical velocity, c) to e) Thomsen parameters ϵ, δ, and γ. Blue lines represent the actual model, red lines the mean value after 100 annealing iterations, and the shaded areas the standard deviation.

by solving a non-linear inversion problem, in which the objective function is

$$\Phi(x_s, y_s, z_s) = \left\{ \frac{1}{N_R} \left[\|(\Delta \mathbf{t}^{cal} - \Delta \mathbf{t}^{obs})_{P-SV}\|_2^2 + \|(\Delta \mathbf{t}^{cal} - \Delta \mathbf{t}^{obs})_{P-SH}\|_2^2 + \|(\Delta \mathbf{t}^{cal} - \Delta \mathbf{t}^{obs})_{SV-SH}\|_2^2 \right] \right\}^{1/2}, \tag{9}$$

where N_R is the number of receivers, x_s, y_s and z_s are the spatial coordinates of the source, and $\Delta \mathbf{t}^{cal}$ and $\Delta \mathbf{t}^{obs}$ are the calculated and observed arrival times differences, respectively, for pairs of seismic phases. The use of arrival time differences between two phases of the same microseismic event allows us to remove the origin time from the calculations, reducing the number of unknowns by one and the non-uniqueness problem associated with this new inverse problem. Often, the origin time is also to be determined during a fracturing process, but falls out of the scope of this analysis. We use VFSA to find the global minimum of the above objective function, where the unknowns are the spatial coordinates of the sources.

The solution of this inversion problem depends on the distance of the event from the monitoring array and its depth. When the monitoring array is vertical and the subsurface is represented by a VTI model, every point of a horizontal circle centered in the monitoring well coordinates is a possible solution, so further information is needed to locate the events in the 3D space (Lagos et al., 2014). This additional information is the backazimuth of each event, which can be calculated from the polarization analysis of the motion components (waveforms) of the phase arrivals. For a single vertical monitoring well, the determination of the backazimuth is one of the main contributors to the uncertainties in the microseismic event location problem (Eisner et al., 2009). It was also mentioned that the difficulty of determining the arrival times of the different phases in a sufficient number of receivers reduce the accuracy on the location. Since our intention here is to analyze only the errors due to the velocity model, the backazimuth and the arrival times are considered to be accurately known for all phases. Also, we are going to assume that there is no relation between the microseismic events, then the localization is carried out independently for each event.

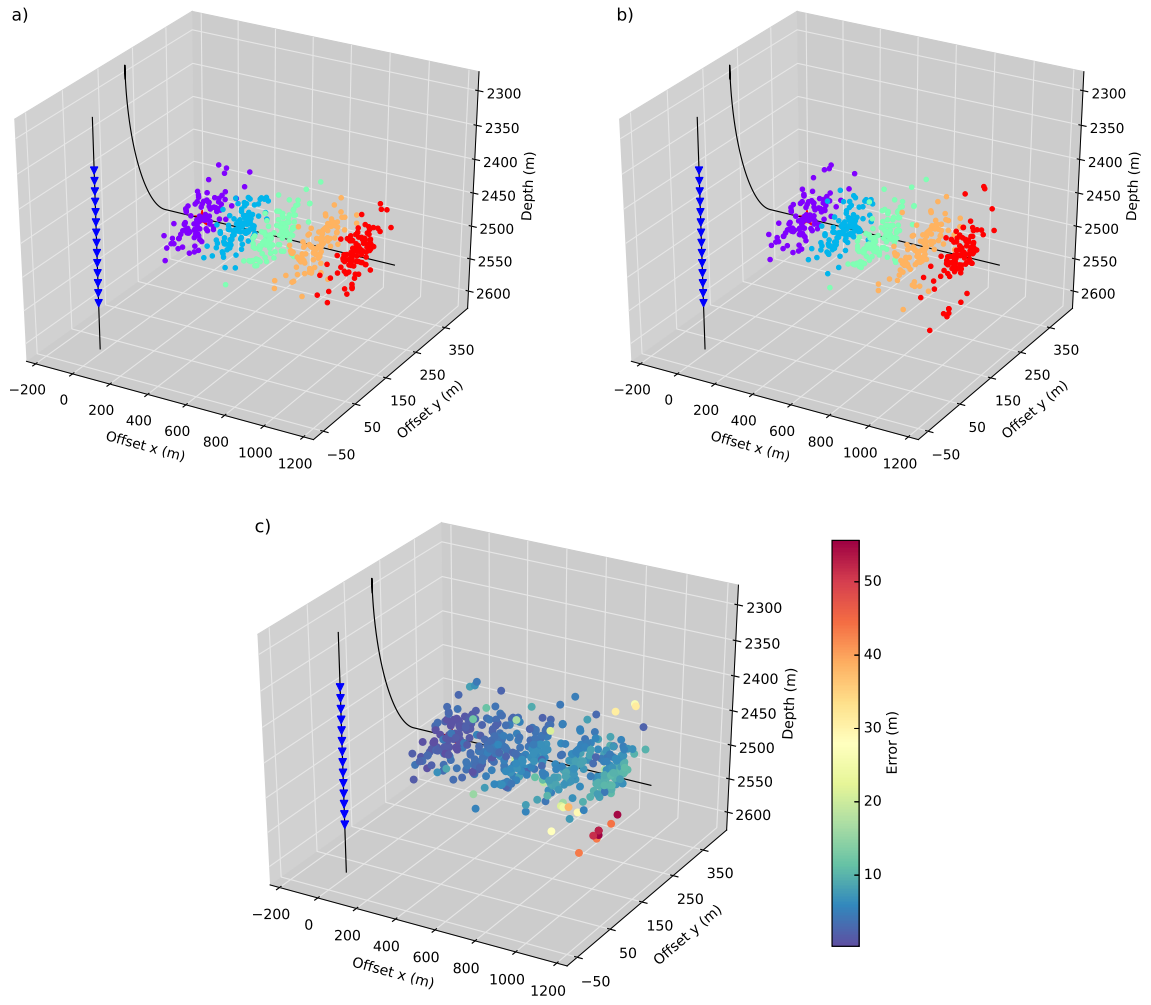

Figure 7: a) Relative position of sources and receivers, b) estimated location of the events, c) error in the estimated event location.

For this example we are going to consider a 3D layered subsurface model, constructed as an extension to the 3D domain of the 1D model used in the previous example and shown in Figure 3. Then we consider a realistically designed situation given by a set of 5 stages of a hydraulic fracture procedure taking place in a horizontal treatment well within the reservoir, i.e. between 2440 m and 2500 m in depth. A total of 100 microseismic events were triggered at each stage. Figure 7a shows the monitoring and treatment wells, represented by the black lines, and the relative position of sources and receivers, represented by the colored clouds of points and the blue triangles, respectively. Each cloud of points represents a hydraulic fracture stage. The receivers array geometry is similar to the one used in the previous examples, and the monitoring well is located at coordinates $x = 0$ m and $y = 0$ m. The treatment well is located at $y = 200$ m and 2480 m depth, spanning 1200 m in the x coordinate. The stages are separated 200 m from each other, being the first stage at $x = 200$ m. The model calibration was carried out considering a perforation shot at the first stage, placed at $x = 200$ m, $y = 200$ m and $z = 2480$ m. The situation was similar to the one already discussed in Figure 5, obtained from the calibration of the model with a single perforation shot within the reservoir.

The results of the event location are shown in Figure 7b. It can be clearly seen that broadly, the different stages of the hydraulic fracturing process are recognizable, being the localization

of the microseismic events successful, especially for those events closer to the perforation shot. For the furthest stages of the hydraulic stimulation the location errors increase. This expected result is better illustrated in Figure 7c, where the color scale indicates the spatial distance or error between the located and the actual microseismic event. The errors increase with distance because the model was calibrated with a single perforation shot that is close to the well. This limits the accuracy on the determination of the anisotropy parameters, affecting more those rays that travel a greater distance.

4 CONCLUSIONS

In this work we proposed a strategy to calibrate the velocity model and simultaneously estimate the Thomsen anisotropy parameters in the context of microseismic event location. The strategy relies on the use of VFSA to minimize an appropriate non-linear cost function. The use of a stochastic algorithm as simulated annealing allowed us to estimate the uncertainties of the estimated solutions. To test the algorithm we performed three different numerical examples using synthetic data. In the first two examples we calibrated and estimated 1D layered velocity models for two different configurations of seismic sources. In the third example the quality of the estimated models was tested through a microseismic event location simulation.

The two first numerical examples showed that, given the arrival times of the P-, SV- and SH-waves, the proposed strategy is capable of estimating acceptable solutions for the anisotropic velocity model that honors the observed data. Also, it was possible to have an insight of the effect that the incidence angle coverage has in the estimated Thomsen parameters. For both examples the synthetic data were generated using the same subsurface model. In the first example we performed the inversion using data from one seismic source located at half deep of the receivers array. In the second example we carried out the inversion adding data from a shallower second source.

In general, the estimated solutions for the vertical velocities were accurate in both examples, showing in the second one some small improvements. Regarding Thomsen parameters, in the second example the improvements were more remarkable, especially the standard deviation. The parameter ϵ showed an accurate mean estimation in both examples, with an improvement of the standard deviation in the second one. In both examples the estimation of the parameter δ was far from optimal. The mean value showed inaccuracies and the standard deviations were large. Those results were expected, because of the poor sensitivity of the data to this parameter. Finally, γ showed accurate estimation of the mean values for both examples, with a slight improvement in the second one. The standard deviations of this parameter showed a considerable improvement in the second example, especially for the upper layers. This behavior was consequence of the sensitivity that this parameter shows for angles near 90°. Despite some observed inaccuracies, especially for δ, the estimated solutions are useful for solving the location problem, as shown by means of the third numerical example.

In the third example we performed a microseismic even location. The objective of this example was to evaluate the effects of the estimated model inaccuracies in the location. To this end we simulated the arrival times of 5 hydraulic stimulation stages, each one represented by 100 microseismic events. Then, after calibrating and estimating the velocity model using the proposed algorithm, we proceeded to locate the events. Despite the inaccuracies in the estimated model, the event location was successful. The different stages of the hydraulic fracturing process were correctly estimated, especially those closer to the perforation shot. As expected, the inaccuracies lead to errors in the location, and these errors increased with the distance from the events to the receivers. Even so, the differences between the actual and the estimated positions

were relatively small.

5 ACKNOWLEDGMENTS

We are grateful to Consejo Nacional de Investigaciones Científicas y Técnicas (CONICET) and YPF Tencnología S.A. for their support.

6 APPENDIX: VERY FAST SIMULATED ANNEALING

Simulated Annealing (SA) is an iterative stochastic algorithm designed to estimate quasi-optimum solutions of hard optimization non-linear problems. The algorithm is derived from the statistical mechanics, an it is named after the annealing process, a metallurgical technique consisting of heating and cooling a metallic material to change its physical properties (e.g. hardness, ductility, etc.). Metropolis et al. (1953) presented a Monte Carlo technique to study the evolution of the physical properties of a solid material at a given temperature. Three decades later (Kirkpatrick et al., 1983) generalized the technique and applied it to the non-linear electronic engineering problem of very large scale integration (VLSI). The unknown parameters of the model play the role of the particles of the metallic material, and the energy state of the system is represented by a cost function. At each iteration step of the SA the model space is randomly perturbed following a predefined probability density function that depends on a control parameter known as temperature. When the temperature is high, the space of possible models is explored in an approximately uniform way. On the other hand, at low temperatures the models associated to the smaller values of the cost function are chosen. This new model is accepted, or rejected, according to the Metropolis criterion. This criterion states that the new model is accepted without conditions if the cost function decreases. On the other hand, if the cost function increases the model is accepted with a non zero probability. This strategy allows the algorithm to accept solutions that increase the cost function, thus avoiding getting trapped in local minimum. The control of the temperature parameter is fundamental to achieve the convergence to the optimal solution. The temperature should be slowly decreased during the optimization process, following a preset cooling schedule. If the temperature is reduced too fast, the particles of the material, represented by the unknown parameters of the model, would not reach the state of minimum energy, represented by the global minimum of the cost function. Finally, the acceptance probability depends on the cost function and the temperature. The lower the cost function, the higher the probability, and vice versa. Convergence is achieved when, at low temperatures, there is no significant decrease in the cost function and the system is in the lowest energy state.

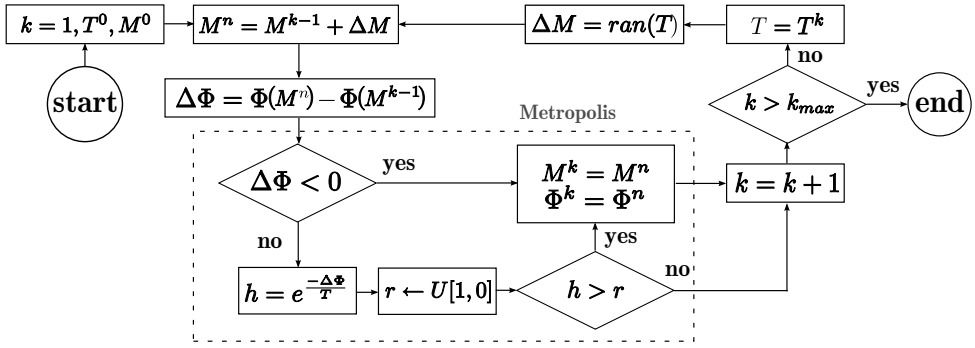

Figure 8: Workflow of Very Fast Simulated Annealing. Φ is the cost function, M^k is the model at the k-iteration and M^n is the temporary model with acceptance probability h.

Ingber (1989) proposed a variation of the SA known as the Very Fast Simulated Annealing (VFSA), which allows a faster cooling schedule and a faster convergence. VFSA uses a long-tailed Cauchy-like distribution that allows to explore the model space in a more efficient way than using Gaussian or uniform distributions as in other conventional SA algorithms. This allows to select a faster cooling schedule to accelerate convergence without limiting the capacity of the algorithm to escape from local minimum. Figure 8 shows the workflow of the VFSA. VFSA is, in some cases, even more efficient than evolutionary methods such as Genetic Algorithms (Ingber and Rosen, 1992).

REFERENCES

Aki K. and Richards P. *Quantitative seismology: theory and methods*. W.H. Freeman and Co., 1980.

Akram J. and Eaton D. Impact of velocity model calibration on microseismic locations. In *SEG Technical Program Expanded Abstracts 2013*, pages 1982–1986. 2013.

Akram J. and Eaton D.W. A review and appraisal of arrival-time picking methods for downhole microseismic data. *Geophysics*, 81(2):KS71–KS91, 2016.

Bachrach R. Linearized orthorhombic avaz inversion: Theoretical and practical consideration. In *SEG Technical Program Expanded Abstracts 2014*, pages 528–532. 2014.

Backus G.E. Long-wave elastic anisotropy produced by horizontal layering. *Journal of Geophysical Research*, 67(11):4427–4440, 1962.

Bardainne T. and Gaucher E. Constrained tomography of realistic velocity models in microseismic monitoring using calibration shots. *Geophysical Prospecting*, 58(5), 2010. ISSN 1365-2478.

Berryman J.G. Long-wave elastic anisotropy in transversely isotropic media. *Geophysics*, 44(5):896–917, 1979.

Berryman J.G., Grechka V.Y., and Berge P.A. Analysis of thomsen parameters for finely layered vti media. *Geophysical Prospecting*, 47(6):959–978, 1999.

Chen H., Zhang G., and Yin X. Avaz inversion for elastic parameter and fracture fluid factor. In *SEG Technical Program Expanded Abstracts 2012*, pages 1–5. 2012.

Cooke D. and Schneider W. Generalized linear inversion of reflection seismic data. *Geophysics*, 48(6):665–676, 1983. doi:10.1190/1.1441497.

Djikpesse H.A. C_{13} and thomsen anisotropic parameter distributions for hydraulic fracture monitoring. *Interpretation*, 3(3):SW1–SW10, 2015.

Downton J. and Gray D. AVAz parameter uncertainty estimation. In *SEG Technical Program Expanded Abstracts 2006*, pages 234–238. 2006.

Eisner L., Duncan P.M., Heigl W.M., and Keller W.R. Uncertainties in passive seismic monitoring. *The Leading Edge*, 28(6):648–655, 2009.

Ingber L. Very fast simulated re-annealing. *Journal of Mathematical Computation and Modelling*, 12:967–973, 1989.

Ingber L. and Rosen B. Genetic algorithms and very fast simulated reannealing: a comparison. *Journal of Mathematical Computation and Modelling*, 16:87–100, 1992.

Kirkpatrick S., Gellat C.J., and Vecchi M. Optimization by simulated annealing. *Science*, 220:671–680, 1983.

Lagos S.R., Sabbione J.I., and Velis D.R. Very fast simulated annealing and particle swarm optimization for microseismic event location. In *Expanded Abstracts*, pages 2188–2192. Society of Exploration Geophysicists, 2014.

Lay T. and Wallace T.C. *Modern Global Seismology*, volume 58. Academic Press, 1995.

Li J., Li C., Morton S.A., Dohmen T., Katahara K., and Toksöz M.N. Microseismic joint location and anisotropic velocity inversion for hydraulic fracturing in a tight bakken reservoir. *Geophysics*, 79(5):C111–C122, 2014.

Liu E. and Martinez A. *Seismic Fracture Characterization, Concepts and Practical Applications*. EAGE, 2012.

Mahmoudian F., Margrave G.F., Wong J., and Henley D.C. Fracture orientation and intensity from avaz inversion: A physical modeling study. In *SEG Technical Program Expanded Abstracts 2013*, pages 483–487. 2013.

Maxwell S. Microseismic location uncertainty. In *CSEG Recorder*, pages 177–188. 2009.

Maxwell S. *Microseismic Imaging of Hydraulic Fracturing*. Society of Exploration Geophysicists, 2014.

Maxwell S., Bennett L., Jones M., and Walsh J. *Anisotropic velocity modeling for microseismic processing: Part 1-Impact of velocity model uncertainty*, chapter 420, pages 2130–2134. SEG, 2010.

Metropolis N., Rosenbluth A., Rosenbluth M., Teller A., and Teller E. Equation of state calculations by fast computing machines. *Journal of Chemical Physics*, 21:1087–1092, 1953.

Pei D., Carmichael J., Waltman C., and Warpinski N. Microseismic anisotropic velocity calibration by using both direct and reflected arrivals. In *SEG Technical Program Expanded Abstracts 2014*, pages 2278–2282. 2014.

Pei D., Quirein J.A., Cornish B.E., Quinn D., and Warpinski N.R. Velocity calibration for microseismic monitoring: A very fast simulated annealing (vfsa) approach for joint-objective optimization. *Geophysics*, 74(6):WCB47–WCB55, 2009.

Sabbione J.I. and Velis D.R. *An automatic method for microseismic events detection based on earthquake phase pickers*, pages 1–5. 2012.

Sabbione J.I. and Velis D.R. A robust method for microseismic event detection based on automatic phase pickers. *Journal of Applied Geophysics*, 99:42 – 50, 2013.

Sheriff R. *Encyclopedic Dictionary of Exploration Geophysics*. Geophysical Reference Series No. 13. Society of Exploration Geophysicists, 4rd. edition, 2002.

Sivia D.S. *Data Analysis: A Bayesian Tutorial*. Clarendon (Oxford Univ. Press), 2nd edition, 1996.

Tarantola A. *Inverse Problem Theory and Methods for Model Parameter Estimation*. SIAM, 2005. Available at the Web.

Thomsen L. Weak elastic anisotropy. *Geophysics*, 51(10):1954–1966, 1986. doi:10.1190/1.1442051.

Tsvankin I. *Seismic Signatures and Analysis of Reflection Data in Anisotropic Media, Third Edition*. Society of Exploration Geophysicists, 2012.

Tsvankin I. and Grechka V. *Seismology of Azimuthally Anisotropic Media and Seismic Fracture Characterization*. Society of Exploration Geophysicists, 2011.

Velis D., Sabbione J.I., and Sacchi M.D. Fast and automatic microseismic phase-arrival detection and denoising by pattern recognition and reduced-rank filtering. *Geophysics*, 80(6):WC25–WC38, 2015.

Velis D.R. Estimating the distribution of primary reflection coefficients. *Geophysics*, 68(4):1417–1422, 2003.

Walden A. and Hosken J. The nature of the non-Gaussianity of primary reflection coefficients and its significance for deconvolution. *Geophysical Prospecting*, 34:1038–1066, 1986.

Warpinski N.R., Sullivan R.B., Uhl J., Waltman C., and Machovoie S. Improved microseismic fracture mapping using perforation timing measurements for velocity calibration. *SPE*

Journal, 10(1):14–23, 2005.

Yilmaz O. *Seismic Data Analysis: processing, inversion, and interpretation of seismic data*. Investigations in Geophysics. Society of Exploration Geophysicists, 2001.

Yue T. and Xiao-fei C. A rapid and accurate two-point ray tracing method in horizontally layered velocity model. *Acta Seismologica Sinica*, 18(2):154–161, 2005.